Multivariate Modeling and Adaptive Control of Autonomous Ferries

Andreas Aurlien* **Morten Breivik*** **Bjørn-Olav H. Eriksen***

** Centre for Autonomous Marine Operations and Systems, Department of Engineering Cybernetics, Norwegian University of Science and Technology (NTNU), N0-7491 Trondheim, Norway.*
E-mail: andreas@aurlien.net, morten.breivik@ieee.org, bjorn-olav.holtung.eriksen@ntnu.no

Abstract: This paper deals with the design and evaluation of a multivariate-based adaptive controller for marine surface vessels. The goal is to make a system that periodically updates the vessel model, used by a dynamic positioning (DP) controller, in order to improve the motion-control performance. The model is generated by analyzing velocity and acceleration data using multivariate analysis (MVA) to fit a 3 degrees of freedom (DOF) surface vessel model. Full-scale experimental results with the prototype autonomous passenger ferry milliAmpere show that the adaptive control system works as intended, and manages to make significant improvements in all performance metrics compared to a non-adaptive control system. The results also show that the system is robust even with the impact of unmeasured wind and wind gusts.

Keywords: Autonomous ferries, Multivariate analysis, Model-based control, Adaptive control.

1. INTRODUCTION

Autopilots for ships have existed since 1922 (Roberts, 2008), but efforts to develop autonomous ships have really only started during the last five years, inspired by the ongoing developments in the automotive industry. In particular, the growing transportation needs in cities and urban areas have sparked the idea to further utilize waterways for transportation of passengers Reddy et al. (2019). This underutilized transportation alternative can be taken advantage of by e.g. developing small, environmentally-friendly autonomous passenger ferries as an additional mobility mode. Such efforts are currently underway at the Norwegian University of Science and Technology (NTNU), where the autonomous ferry prototype milliAmpere has been in operation since 2017, see Fig. 1. The milliAmpere is an all-electric R&D platform used to develop and test algorithms for autonomous operation, including situational awareness algorithms, motion control systems such as dynamic positioning (DP), thrust allocation algorithms, motion planning, collision avoidance, docking, etc. In 2021, a larger ferry version named milliAmpere 2 will be launched by NTNU and its partners, which is intended to carry up to 12 passengers in regular traffic between Ravnkloa and Fosenkaia in the Trondheim city canal. As part of this R&D effort, the NTNU spinoff company Zeabuz was established in 2019, which aims to deliver its first commercially available autonomous passenger ferry system in 2022, exactly 100 years after the birth of the ship autopilot.

When controlling autonomous urban passenger ferries, using a DP system for low-speed applications is highly relevant. In particular, a DP system delivering robust and precise performance is required, which is something that the higher levels in the autonomy stack must rely on. In this regard, a model-based DP controller as part of the DP system represents a traditional design choice. A perfect model is, however, impossible to obtain. Several assumptions and approximations are made to obtain a simplified model of a vessel. In many cases, this results in a good enough model for control purposes. However, an imperfect model will result in sub-optimal control actions, which can result in energy-inefficient and imprecise maneuvers. As such, it is important to not disregard or overlook the value of sensor data that can be used to obtain a better model.

The development of the emerging field of big data cybernetics (BDC) is a new effort also currently underway at NTNU (Martens, 2015). The goal of BDC is to combine the best of theory-driven and data-driven modeling methods in order to create continuously evolving system models in terms of both parameters and variables, a sort of "Kalman filter 2.0". In BDC, multivariate analysis (MVA) is a fundamental basis for being able to model unmodeled dynamics by analyzing sensor data, which can give an estimate of the model error. The concept is that the MVA finds a correlation in the data that best describes the model error. With this kind of analysis, an adaptive control system for updating the model can be developed, reducing the inconsistency observed in the gathered data. This approach to develop an adaptive control system is the core focus and main contribution of this paper. Other contributions include the experimental setup and carrying out of full-scale experiments with milliAmpere to validate the proposed adaptive control system.

Specifically, the design of an adaptive control system which used available sensor data to improve the milliAmpere model was started by the work of Jervan (2020), while Aurlien (2021) continued the work to update the control system and test its closed-loop performance in full scale. As such, we have used Gale et al. (2017)'s improvement

Fig. 1. The milliAmpere ferry prototype right after the launching.

of a robotic manipulator model as the basis of this work. An important motivation for this paper is to share the design of the proposed adaptive control system and how it performs compared to a non-adaptive control system. Finally, other schemes for system identification and adaptive control can be found in e.g. (Lennart, 1999) and (Eugene et al., 2013) and the references therein, respectively.

The remainder of this paper is structured as follows: Section 2 introduces the surface vessel model, while Section 3 shows how we can use such a model to obtain precise and efficient motion control. The core part of the adaptive control system that builds on MVA gets introduced in in Section 4. Section 5 describes the experimental setup and illustrates the improvements in performance due to the proposed adaptive system. Finally, Section 6 concludes the paper.

2. SURFACE VESSEL MODEL

The motion of a surface vessel can with the Society of Naval Architects and Marine Engineers (SNAME) notation be represented by the pose vector $\boldsymbol{\eta} = [x, y, \psi]^\top \in \mathbb{R}^2 \times \mathbb{S}$ and the velocity vector $\boldsymbol{\nu} = [u, v, r] \in \mathbb{R}^3$. Here (x, y) is the Cartesian position and ψ is the yaw angle, both given in a local north-east-down (NED) frame. Furthermore, (u, v) is the linear velocity given in the body-fixed frame, and r is the yaw rate.

Fossen (2011) models the 3-degrees of freedom (DOF) dynamics of a surface vessel as:

$$\dot{\boldsymbol{\eta}} = \boldsymbol{R}(\psi)\boldsymbol{\nu} \tag{1}$$

$$\boldsymbol{M}^*\dot{\boldsymbol{\nu}} + \boldsymbol{C}^*(\boldsymbol{\nu})\boldsymbol{\nu} + \boldsymbol{D}^*(\boldsymbol{\nu})\boldsymbol{\nu} = \boldsymbol{\tau}^* + \boldsymbol{R}^\top(\psi)\boldsymbol{w}^*, \tag{2}$$

where

$$\boldsymbol{R}(\psi) = \begin{bmatrix} cos(\psi) & -sin(\psi) & 0 \\ sin(\psi) & cos(\psi) & 0 \\ 0 & 0 & 1 \end{bmatrix} \tag{3}$$

is a rotation matrix $\boldsymbol{R} \in SO(3)$, and where $\boldsymbol{M}^*$, $\boldsymbol{C}^*$, $\boldsymbol{D}^*$, and $\boldsymbol{\tau}^*$ are the real inertia matrix, Coriolis and centripetal matrix, damping matrix, and control input vector, respectively. The Cartesian vector $\boldsymbol{w}^*$ in the NED reference frame models the real force disturbances which include environmental forces such as wind and current. In the model, the system matrices are assumed to satisfy the properties $\boldsymbol{M}^* = \boldsymbol{M}^{*\top} > 0$, $\boldsymbol{C}^*(\boldsymbol{\nu}) = -\boldsymbol{C}^*(\boldsymbol{\nu})^\top$, and $\boldsymbol{D}^*(\boldsymbol{\nu}) > 0$. The model will, however, never be perfect. The model error can be expressed as:

$$\boldsymbol{M}^* = \frac{1}{\delta}\boldsymbol{M} \tag{4}$$

$$\boldsymbol{C}^*(\boldsymbol{\nu}) = \frac{1}{\delta}\boldsymbol{C}(\boldsymbol{\nu}) \tag{5}$$

$$\boldsymbol{D}^*(\boldsymbol{\nu}) = \frac{1}{\sigma}\boldsymbol{D}(\boldsymbol{\nu}) \tag{6}$$

$$\boldsymbol{\tau}^* = \frac{1}{\rho}\boldsymbol{\tau}, \tag{7}$$

where $^/*$ denotes the actual dynamics, $\delta \in \mathbb{R}^+$ expresses the error associated with the inertia and Coriolis matrices, $\sigma \in \mathbb{R}^+$ expresses the error associated with the damping matrix, and $\rho \in \mathbb{R}^+$ is the error associated with the control input vector. The goal of the adaptive controller is to minimize this model error. An imprecise model with system matrices $\mathbf{M}$, $\mathbf{C}$, and $\mathbf{D}$ can be generated by considering a good model as the left hand side of (4), (5), and (6) and selecting δ and σ different to one.

3. MOTION CONTROL

Fig. 2 shows a flow chart of how a motion control system can be designed. A guidance system provides waypoints that when combined maps out a path for the vessel to follow. A third-order reference filter then generates a smooth trajectory between the waypoints consisting of desired values for position, velocity, and acceleration. The DP controller then uses the desired values and measurements to maintain the desired trajectory. The control signal from the DP controller is processed by a thruster allocation algorithm that distributes the desired control forces and moment to the available vessel thrusters.

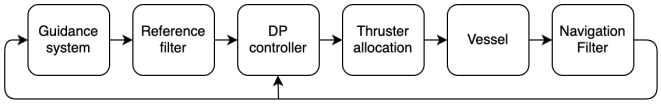

Fig. 2. Flow chart for achievement of motion control.

3.1 Dynamic Positioning

A DP controller's task is usually to maintain a ship's position and heading. However, the velocity can also be controlled by including a velocity reference in the controller. A DP controller can be implemented as a PID feedback (FB) controller and a feed-forward (FF) controller. The PID controller is defined as

$$\boldsymbol{\tau}_{PID} = -\boldsymbol{R}^\top(\psi)\boldsymbol{K}_p(\boldsymbol{\eta} - \boldsymbol{\eta}_d) - \boldsymbol{K}_d(\boldsymbol{\nu} - \boldsymbol{\nu}_d) - \boldsymbol{R}^\top(\psi)\boldsymbol{K_i}\int_0^t (\boldsymbol{\eta} - \boldsymbol{\eta}_d)dt, \tag{8}$$

where $\boldsymbol{K}_p, \boldsymbol{K}_i, \boldsymbol{K}_d \in \mathbb{R}^{3\times3}$ are design gain matrices with $\boldsymbol{K}_p, \boldsymbol{K}_i, \boldsymbol{K}_d \geq 0$ and $\boldsymbol{\nu}_d \in \mathbb{R}^3$ is the desired velocity vector. To improve the performance, we also use a FF controller which is defined as

$$\boldsymbol{\tau}_{FF} = \boldsymbol{F}(\dot{\boldsymbol{\nu}}_d, \boldsymbol{\nu}_d), \tag{9}$$

where

$$\boldsymbol{F}(\dot{\boldsymbol{\nu}}, \boldsymbol{\nu}) = \boldsymbol{M}\dot{\boldsymbol{\nu}} + \boldsymbol{C}(\boldsymbol{\nu})\boldsymbol{\nu} + \boldsymbol{D}(\boldsymbol{\nu})\boldsymbol{\nu} - \boldsymbol{R}^\top(\psi)\boldsymbol{w} \tag{10}$$

is the surface vessel model. The total DP controller then becomes:

$$\boldsymbol{\tau} = \boldsymbol{\tau}_{FF} + \boldsymbol{\tau}_{PID}, \tag{11}$$

which makes it possible to achieve the control objective $\lim_{t\to\infty}(\boldsymbol{\eta} - \boldsymbol{\eta}_d) = 0$.

4. MULTIVARIATE ANALYSIS

An improved vessel model can be obtained by checking for model inconsistency in the vessel state measurements. Partial least squares (PLS) regression can be used to find underlying structures between two data sets. For the data sets $\boldsymbol{X} \in \mathbb{R}^{N\times K}$ and $\boldsymbol{Y} \in \mathbb{R}^{N\times k}$, where k is the number of output dimensions, K is the number of input dimensions, and N is the number of samples, the goal is to predict $\boldsymbol{Y}$ with a linear combination of $\boldsymbol{X}$ according to

$$\hat{\boldsymbol{Y}} = [\mathbf{1}, \boldsymbol{X}]\boldsymbol{\beta}, \tag{12}$$

where $\mathbf{1} \in \mathbb{R}^{N\times 1}$ is a vector and $\boldsymbol{\beta} \in \mathbb{R}^{K+1\times k}$ is a matrix. The correlation between $\boldsymbol{X}$ and $\boldsymbol{Y}$ is maximized so that the residual $\boldsymbol{E}$ in

$$\boldsymbol{Y} = [\mathbf{1}, \boldsymbol{X}]\boldsymbol{\beta} + \boldsymbol{E}, \tag{13}$$

is minimized. This means that white noise will not affect the analysis, since there is no correlation in white noise. The simple partial least squares (SIMPLS) algorithm can be used to solve the PLS regression problem (De Jong, 1993).

Storing and analysing the error between model-predicted and real motion can lead to an improved vessel model. The lack-of-fit residual is a measure of the unmodeled forces acting on a surface vessel. It is defined as

$$\boldsymbol{\tau}_\epsilon \triangleq \boldsymbol{\tau} - \hat{\boldsymbol{\tau}}, \tag{14}$$

where

$$\hat{\boldsymbol{\tau}} = \boldsymbol{F}(\dot{\boldsymbol{\nu}}_{mes}, \boldsymbol{\nu}_{mes}) \tag{15}$$

is the estimated applied force, while $\dot{\boldsymbol{\nu}}_{mes}, \boldsymbol{\nu}_{mes} \in \mathbb{R}^3$ are the measured vessel acceleration and velocity, respectively.

With MVA, the lack-of-fit residual is modeled as

$$\boldsymbol{\tau}_\epsilon \approx \boldsymbol{\theta}^\top \boldsymbol{\phi}, \tag{16}$$

where $\boldsymbol{\phi} \in \mathbb{R}^{b\times 1}$ contains the selected basis functions, $\boldsymbol{\theta} \in \mathbb{R}^{b\times 3}$ is the scores of the selected basis functions, and b is the number of basis functions. Comparing this lack-of-fit residual with (12), where samples have been collected over a period of time, we have $\boldsymbol{\phi} \in \mathbb{R}^{(K+1)\times N} = [\mathbf{1}, \boldsymbol{X}]^\top$ and $\boldsymbol{\theta} = \boldsymbol{\beta}^\top$.

Better estimates of the parameters describing the model of Fossen (2011) can be made by adding each term in the model as a basis function in the MVA. The basis functions that describe the 3-DOF model of Fossen (2011) without disturbances are

$$\boldsymbol{\phi}_1 = [\dot{u}, \dot{v}, \dot{r}, uv, ur, vr, rr, u, v, r, sgn(u)u^2, sgn(v)v^2, sgn(r)r^2, u^3, v^3, r^3, |u|u, |v|v, |r|r|v|r, |r|v]^\top. \tag{17}$$

The remaining components in the lack-of-fit residual, such as current and wind impact, should be modeled by other basis functions. According to Blendermann (1994), the wind will apply a force to a 3-DOF ship model in the following manner:

$$\boldsymbol{\tau}_{wind} = \frac{1}{2}\rho_a V_{rw}^2 \begin{bmatrix} C_X(\gamma_{rw})A_{F_w} \\ C_Y(\gamma_{rw})A_{L_w} \\ C_N(\gamma_{rw})A_{L_w}L_{0a} \end{bmatrix}, \tag{18}$$

where ρ_a is the air density, $V_{rw} \in \mathbb{R}$ is the relative air speed, γ_{rw} is the angle of attack of V_{rw} relative to the bow of the ship, $C_X(\gamma_{rw}), C_Y(\gamma_{rw})$, and $C_N(\gamma_{rw})$ are the wind coefficients for horizontal plane motion, L_{0a} is the overall length, and A_{F_w} and A_{L_w} are the frontal and lateral projected areas, respectively. The basis functions

$$\boldsymbol{\phi}_2 = [V_{rw}^2 cos(\gamma_{rw}), V_{rw}^2 sin(\gamma_{rw}), V_{rw}^2 sin(\gamma_{rw})\gamma_{rw}]^\top, \tag{19}$$

are good linear approximations to the Blendermann wind model. If wind is measured, the basis functions are added to the MVA. In simulations done by Aurlien (2020), $\boldsymbol{\phi}_2$ detects most of the wind contribution in the lack-of-fit residual. Similarly, we can use the basis functions

$$\boldsymbol{\phi}_3 = [V_{rc}^2 cos(\gamma_{rc}), V_{rc}^2 sin(\gamma_{rc}), V_{rc}^2 sin(\gamma_{rc})\gamma_{rc}]^\top, \tag{20}$$

where $V_{rc} \in \mathbb{R}$ is the relative current, γ_{rc} is the angle of attack of V_{rc} relative to the bow of the ship, to model the current if we add current measurements. The basis functions take inspiration from the Blendermann (1994) model. With these basis functions we assume uniform flow around the ship. This assumption is justified for relatively small ships. All basis functions are gathered according to

$$\boldsymbol{\phi} = [\boldsymbol{\phi}_1^\top, \boldsymbol{\phi}_2^\top, \boldsymbol{\phi}_3^\top]^\top. \tag{21}$$

The advantage of describing the lack-of-fit residual as done in (14) is that an adaptively improved vessel model can be described as

$$\boldsymbol{F}_P(\dot{\boldsymbol{\nu}}, \boldsymbol{\nu}, \boldsymbol{\phi}) = \boldsymbol{M}\dot{\boldsymbol{\nu}} + \boldsymbol{C}\boldsymbol{\nu} + \boldsymbol{D}\boldsymbol{\nu} + \boldsymbol{\theta}_P^\top \boldsymbol{\phi}, \tag{22}$$

where P denotes the P^{th} model update. The FF control signal from (9) is now updated to

$$\boldsymbol{\tau}_{FF} = \boldsymbol{F}_P(\dot{\boldsymbol{\nu}}_d, \boldsymbol{\nu}_d, \boldsymbol{\phi}_d), \tag{23}$$

where $\boldsymbol{\phi}_d = [\boldsymbol{\phi}_{1_d}^\top, \boldsymbol{\phi}_{2_{mes}}^\top, \boldsymbol{\phi}_{3_{mes}}^\top]^\top$. The estimated applied force are similarly updated according to

$$\hat{\boldsymbol{\tau}} = \boldsymbol{F}_P(\dot{\boldsymbol{\nu}}_{mes}, \boldsymbol{\nu}_{mes}, \boldsymbol{\phi}_{mes}). \tag{24}$$

The static terms in (22) are referred to as the base model which is the model that the system is initiated with. The adaptive term $\boldsymbol{\theta}_P^\top \boldsymbol{\phi}$ is the lack-of-fit model P that is added and updated to express the difference between the base model and the observed dynamics.

A slower model update loop is introduced by redefining the base model as

$$\boldsymbol{F}(\dot{\boldsymbol{\nu}}, \boldsymbol{\nu}, \boldsymbol{\phi}) = \frac{1}{S}\sum_{P=1}^{S} \boldsymbol{F}_P(\dot{\boldsymbol{\nu}}, \boldsymbol{\nu}, \boldsymbol{\phi}) \tag{25}$$

where S is a predefined constant for number of models to average. The slow model update will ensure that the system always is booted with a good dynamics model. Fig. 3 shows how the improved model is used as a part in the DP controller. The block diagram in Fig. 4 shows how the improved model is generated by providing the lack-of-fit residual and the basis functions for the MVA. In Fig. 4, $\boldsymbol{\alpha}_{mes} \in \mathbb{R}^{2\times 1}$ are the measured thuster rpm and angle, respectively.

5. EXPERIMENTAL RESULTS AND PERFORMANCE EVALUATION

5.1 Experimental setup

Full-scale experiments are designed for the ferry prototype milliAmpere to verify the adaptive controller. The vessel

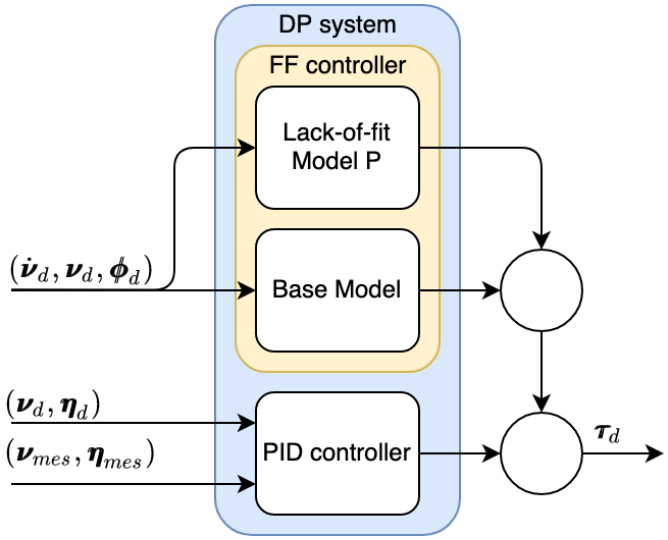

Fig. 3. A block diagram of the DP controller.

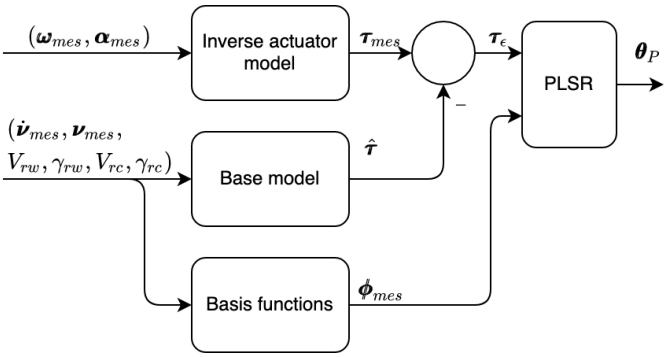

Fig. 4. A block diagram showing the generation of the improved model.

has a length of 5 m, a beam of 2.8 m and weighs 1670 kg. Two azimuth thrusters, delivering 2 kW each, control the movement of the ferry. The hull of milliAmpere is symmetrical both around the x and y axes and is flat underneath. The lack of a keel makes milliAmpere turn quickly, but also makes it unstable in yaw. When assuming symmetry along the x-axis, the inertia matrix is given as

$$\begin{aligned} \boldsymbol{M}^* &\triangleq \boldsymbol{M}_{RB} + \boldsymbol{M}_A \\ &= \begin{bmatrix} m_{11} & 0 & 0 \\ 0 & m_{22} & m_{23} \\ 0 & m_{32} & m_{33}. \end{bmatrix} \end{aligned} \tag{26}$$

The Coriolis and centripetal matrix is given as

$$\begin{aligned} \boldsymbol{C}^*(\boldsymbol{\nu}) &\triangleq \boldsymbol{C}_{RB}(\boldsymbol{\nu}) + \boldsymbol{C}_A(\boldsymbol{\nu}) \\ &= \begin{bmatrix} 0 & 0 & c_{13}(\boldsymbol{\nu}) \\ 0 & 0 & c_{23}(\boldsymbol{\nu}) \\ -c_{13}(\boldsymbol{\nu}) & -c_{23}(\boldsymbol{\nu}) & 0 \end{bmatrix} \end{aligned} \tag{27}$$

where $c_{13}(\boldsymbol{\nu}) = Y_{\dot{v}} v + \frac{1}{2}(N_{\dot{v}} + Y_{\dot{r}})$ and $c_{23}(\boldsymbol{\nu}) = -X_{\dot{u}} u$. Finally, the damping matrix is given as

$$\begin{aligned} \boldsymbol{D}^*(\boldsymbol{\nu}) &\triangleq \boldsymbol{D}_L + \boldsymbol{D}_{NL}(\boldsymbol{\nu}) \\ &= \begin{bmatrix} -d_{11}(\boldsymbol{\nu}) & 0 & 0 \\ 0 & -d_{22}(\boldsymbol{\nu}) & -d_{23}(\boldsymbol{\nu}) \\ 0 & -d_{32}(\boldsymbol{\nu}) & -d_{33}(\boldsymbol{\nu}) \end{bmatrix}, \end{aligned} \tag{28}$$

where $d_{11}(\boldsymbol{\nu}) = X_u + X_{|u|u}|u| + X_{uuu}u^2$, $d_{22}(\boldsymbol{\nu}) = Y_v + Y_{|v|v}|v| + Y_{|r|v}|r|, d_{23}(\boldsymbol{\nu}) = Y_r + Y_{|v|r}|v| + Y_{|r|r}|r| + Y_{vvv}v^2$,

Table 1. Estimated model parameters for milliAmpere (Pedersen, 2019).

Parameter	Value	Parameter	Value
m_{11}	2389.657	$Y_{\|v\|v}$	-116.486
m_{12}	0	Y_{vvv}	-24.313
m_{13}	0	$Y_{\|r\|v}$	-1540.383
m_{21}	0	Y_r	24.732
m_{22}	2533.911	$Y_{\|v\|r}$	572.141
m_{23}	62.386	$Y_{\|r\|r}$	-115.457
m_{31}	0	N_v	3.524
m_{32}	28.141	$N_{\|v\|v}$	-0.832
m_{33}	5068.910	$N_{\|r\|v}$	336.827
X_u	-27.632	N_r	-122.860
$X_{\|u\|u}$	-110.064	$N_{\|r\|r}$	-874.428
X_{uuu}	-13.965	N_{rrr}	0.000
Y_v	-52.947	$N_{\|v\|r}$	-121.957

$d_{32}(\boldsymbol{\nu}) = N_v + N_{|v|v}|v| + N_{|r|v}|r|$ and $d_{33}(\boldsymbol{\nu}) = N_r + N_{|v|r}|v| + N_{|r|r}|r| + N_{rrr}r^2$. The parameter values for $\boldsymbol{M}, \boldsymbol{C}(\boldsymbol{\nu})$ and $\boldsymbol{D}(\boldsymbol{\nu})$ for milliAmpere found by Pedersen (2019) are listed in Table 1.

To compare the performance of the adaptive controller relative to a controller using an imperfect model, we use a 8-corner motion test. This path is used to ensure that the adaptive controller has persistent excitation (PE).

We use a reference filter to generate the trajectory for the DP controller to follow. The reference filter is given by

$$\boldsymbol{\eta}_d^{(3)} + (2\boldsymbol{\Delta} + \boldsymbol{I})\boldsymbol{\Omega}\ddot{\boldsymbol{\eta}}_d + (2\boldsymbol{\Delta} + \boldsymbol{I})\boldsymbol{\Omega}^2\dot{\boldsymbol{\eta}}_d + \boldsymbol{\Omega}^3\boldsymbol{\eta}_d = \boldsymbol{\Omega}^3\boldsymbol{r}, \tag{29}$$

where $\boldsymbol{\Omega}, \boldsymbol{\Delta} \in \mathbb{R}^{3\times3}$ are positive definite design matrices, that determine the dynamics of the filter, and $\boldsymbol{r}$ is the reference setpoint. The outputs of the filter are the reference signals $\boldsymbol{\eta}_d, \dot{\boldsymbol{\eta}}_d$ and $\ddot{\boldsymbol{\eta}}_d$. The reference filter receives

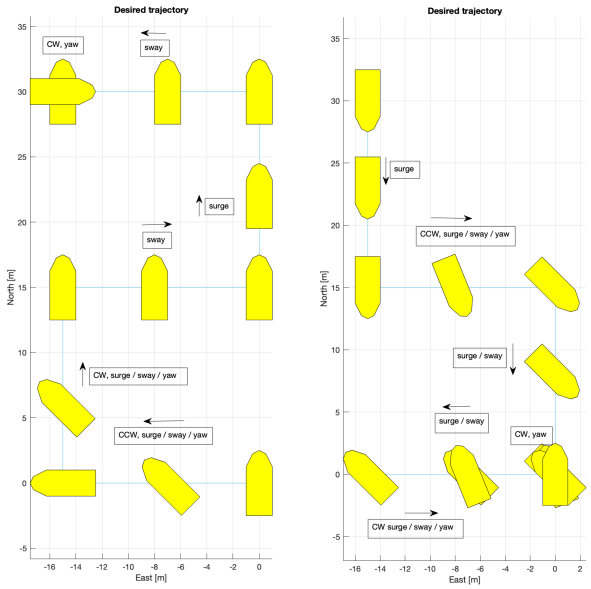

(a) Part one. (b) Part two.

Fig. 5. The calibration path used to excite the adaptive controller.

waypoints with an interval of 60 seconds. We use the pose from all corners of the calibration path showed in Fig. 5 as waypoints. This test is a modified version of the 4-corner test by Skjetne et al. (2017) used by Jervan (2020) in his master's thesis. This 8-corner test moves and turns in all directions in case the symmetry assumption does not hold. The DP controller then uses the desired values for position, velocity and acceleration to follow the trajectory generated by the reference filter.

For the experiments, we initiated the system with an imprecise and scaled version of Pedersen's (2019) model using $\delta = \sigma = 0.4$ and $\rho = 1$. By doing this we ensured that the adaptive system could find a new and better model, in case the model by Pedersen (2019) is good. In the MVA, we use 12 principal components when performing the SIMPLS algorithm. The wind was substantial the day the test was performed, according to the weather forecast 6 m/s and up to 10 m/s in the gusts. The vessel was, however, to some degree sheltered from the wind by the milo in the harbor. The adaptive system suggests a new model once the calibration path is completed, and automatically stores the data and starts a new round. A round is a full cycle of the 8-corner test. Thus, the model used in round 3 is based on data collected in rounds 1 and 2.

5.2 Estimation of acceleration

In order to do the MVA, we need acceleration data for surge, sway and yaw. Since the acceleration data is only used as a part of a training set, we do not need to do the estimation on-line. Since the PLS regression is unaffected by white noise, we can also allow the acceleration estimate to contain white noise. Taking advantage of these relaxing requirements, we use the numerical derivative of smoothed velocity data to estimate the acceleration. Smoothing is a filtering process where we use data not only from the past but also from the future. The convolution

$$\boldsymbol{\nu}_{smoothed}(t) = \boldsymbol{\nu}(t) * \boldsymbol{g}(t) = \int_{-\infty}^{\infty} \boldsymbol{\nu}(\xi)\boldsymbol{g}(t-\xi)d\xi, \quad (30)$$

where $\boldsymbol{g}(t)$ is a square window, describes the smoothing process. In the experiments, we used a window of ± 1.0 seconds for both surge, sway, and yaw where all components of $\boldsymbol{\nu}$ inside the window are weighted equally. The integral of the window is 1, making this an averaging process. We need the smoothing step because the velocity data is no longer white, due to the previous filtration in a navigation filter.

5.3 Performance metrics

To compare the performance of motion controllers for autonomous ferries, it is useful to employ the following metrics: The integral of the square of the error (ISE) defined as

$$ISE = \int_0^t e^2 dt, \quad (31)$$

which penalizes large errors more than small errors, the integral of the absolute error (IAE) that is defined as

$$IAE = \int_0^t |e| dt, \quad (32)$$

which penalizes errors linearly, and the integral of the absolute error multiplied by the energy consumption (IAEW) that is defined as (Sørensen and Breivik, 2015):

$$IAEW = \int_0^t |e(t)|dt \int_0^t P(t)dt, \quad (33)$$

which scales the precision with the power usage. Additionally we use the integral of the energy consumption (IEC), defined as

$$IEC = \int_0^t P(t)dt. \quad (34)$$

The cross-track error e is defined by

$$e = -\sin(\psi)(x - x_d) + \cos(\psi)(y - y_d). \quad (35)$$

5.4 Experimental results

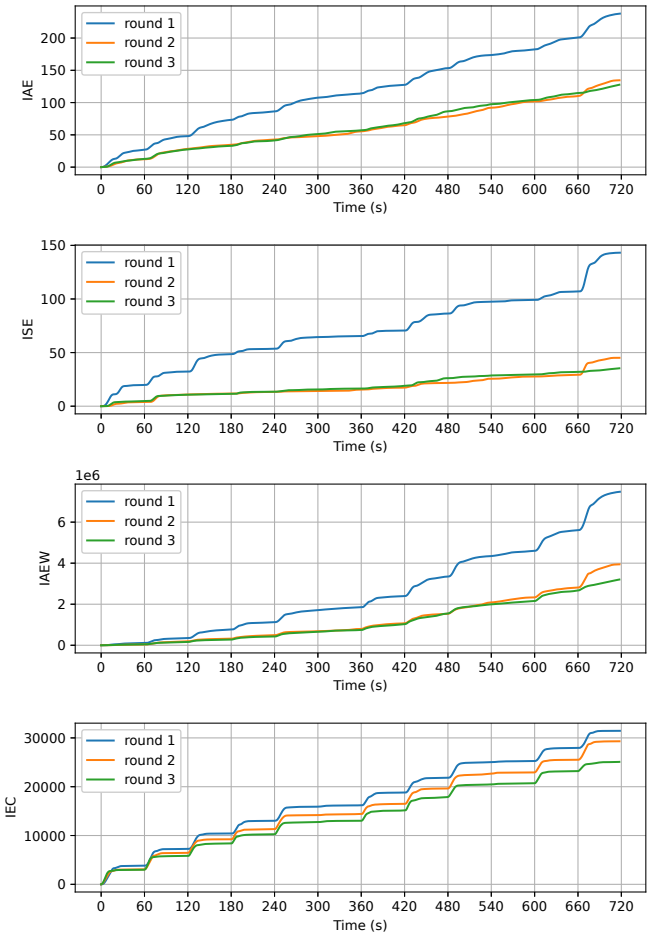

Fig. 6. Performance of the adaptive system in experiments. The model is updated every round based on the data from previous rounds.

Fig. 6 shows how the adaptive model improves the performance for two consecutive rounds as more training data is collected. The difference in the precision between the first and the second model-update is not very big, suggesting that the adaptive model is close to convergence for the current conditions. The results show that the use of the adaptive model in the FF increases the precision and reduces the energy usage. To quantify the results, we find that the IAE, ISE, IAEW, and IEC from round 1 to round 3 are improved by 46%, 75%, 57%, and 20%, respectively.

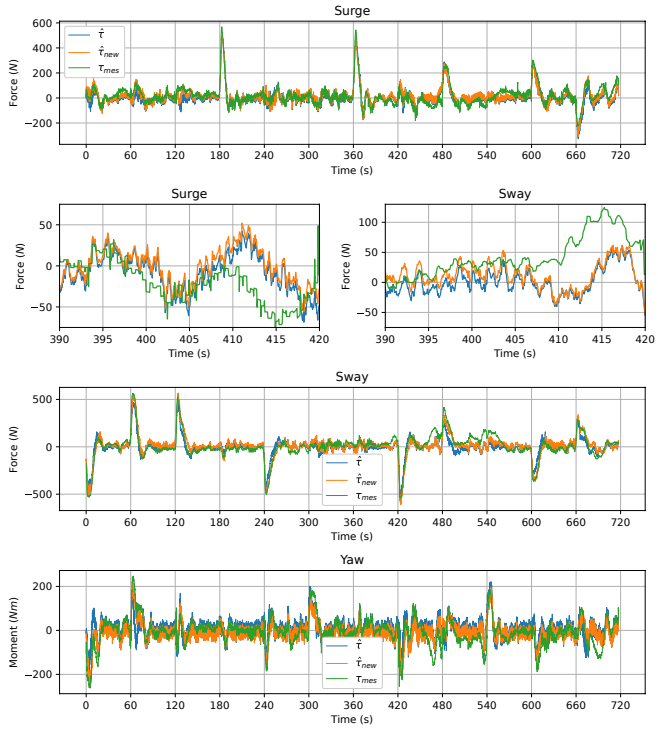

Fig. 7. Model fit for Pedersen's (2019) model and the adaptive model.

Fig. 7 shows how the model reconstructs the estimated actuator force $\boldsymbol{\tau}_{mes}$, based on velocity and acceleration data. Here, $\hat{\boldsymbol{\tau}}$ is estimated using the current model of milliAmpere, which is Pedersen's (2019) model listed in Table 1, while $\hat{\boldsymbol{\tau}}_{new}$ is estimated with the adaptive model found after completing round 2. The model is defined by

$$\hat{\boldsymbol{\tau}}_{new} = \boldsymbol{F}_2(\boldsymbol{\phi}_1) = \begin{bmatrix} 12 & 4 & -13 \\ 2831 & -182 & 78 \\ -124 & 2977 & 185 \\ 81 & 261 & 4802 \\ -25 & 129 & 192 \\ 140 & 1250 & -317 \\ -2071 & 54 & -21 \\ -260 & 172 & 86 \\ 9 & 215 & 33 \\ 20 & 183 & 29 \\ -34 & 145 & 284 \\ 403 & -639 & -96 \\ -19 & 270 & -43 \\ -85 & 309 & 657 \\ -105 & -423 & 831 \\ -163 & 888 & 119 \\ -290 & 432 & 88 \\ 67 & -61 & 7 \\ -11 & 30 & 29 \end{bmatrix}^\top \boldsymbol{\phi}_1, \qquad (36)$$

where all terms of (22) are combined for a more compact representation. We use the mean squared error (MSE) to compare the model fit, which shows that the model error gets improved by 84%, 87%, and 68% for surge, sway and yaw, respectively.

Considering the experimental results, we see that the adaptive system manages to find a better model of the hydrodynamics. However, there are still deviations between the measured and estimated force applied. The most likely explanation for this is that wind gusts have pushed the vessel off its trajectory so that when the vessel applies a counter-force, the vessel stays relatively still. In Fig. 7, we see that all deviations fit a natural compensating force to wind disturbances from the north-west (NW) direction, which was the actual wind direction. At $t = 405\ s$ to $t = 420\ s$ the vessel's heading is $\psi = \pi\ rad$ and tries to keep its pose. Once the wind gust comes from the NW direction, we observe that the models detect the force and that the thrusters try to cancel out the wind impact by applying a force in negative surge and positive sway, which with the current heading is a force in the NW direction. The models then detect the net force that is needed to take the vessel back to its desired pose.

Currents can also be a component of deviations between the measured and estimated force. When currents are present, the ground movement and the relative water movement will no longer be the same.

Since the adaptive system lacks wind and current measurements, we can not expect the model to understand these components. It is therefore a good sign that we observe that the adaptive system does not over-fit the lack-of-fit residual and at the same time finds an improved model of what the system can model.

6. CONCLUSION

We have presented the design of an adaptive control system using position and acceleration data to fit a 3-DOF vessel model using multivariate analysis. Experimental results show that the adaptive system manages to increase the motion control precision and lower the energy usage when the system is initiated with an imprecise model. The adaptive system also proves to be robust against wind impact. The adaptive model obtained in the experiments outperforms the current model of milliAmpere found by Pedersen (2019). Additionally, we have designed the adaptive control system to be flexible for further model improvements if adding measurements from wind and current.

For further work, we need to test how the adaptive system works under normal operations. A concern is that normal operations will not fully excite the adaptive system and therefore suggest imprecise or even wrong model improvements that could lead to worse performance.

We also need research on when it is smart to update the model. On the one extreme, we want to have as much data as possible before making a model update, while on the other hand, updating the model often will account for disturbances such as e.g. changing passenger load. Another factor that needs to be considered is that if too small data sets are used to detect passenger load, we could potentially over-fit static disturbances. A worst-case scenario is if the data set only contains surge movement with $\gamma_{rc} = 0\ rad$. The model generated will then not be able to filter out the current impact in the MVA.

ACKNOWLEDGEMENTS

This work was supported by the NTNU Digital transformation project Autoferry and the Research Council of

Norway through the Centres of Excellence funding scheme, project no. 223254.

REFERENCES

Aurlien, A. (2020). Multivariate modeling and adaptive control of autonomous ferries. Specialization project report. Norwegian University of Science and Technology.

Aurlien, A. (2021). *Multivariate modeling and adaptive control of autonomous ferries*. Master's thesis, Norwegian University of Science and Technology (NTNU), Trondheim, Norway.

Blendermann, W. (1994). Parameter identification of wind loads on ships. *Journal of Wind Engineering and Industrial Aerodynamics*, 51(3), 339–351.

De Jong, S. (1993). SIMPLS: an alternative approach to partial least squares regression. *Chemometrics and intelligent laboratory systems*, 18(3), 251–263.

Eugene, L., Kevin, W., and Howe, D. (2013). Robust and adaptive control with aerospace applications.

Fossen, T.I. (2011). *Handbook of marine craft hydrodynamics and motion control*. John Wiley & Sons.

Gale, S., Rahmati, H., Gravdahl, J.T., and Martens, H. (2017). Improvement of a robotic manipulator model based on multivariate residual modeling. *Frontiers in Robotics and AI*, 4, 28.

Jervan, M. (2020). *Improvement of an autonomous passenger ferry model based on multivariate residual modeling*. Master's thesis, Norwegian University of Science and Technology (NTNU), Trondheim, Norway.

Lennart, L. (1999). System identification: theory for the user. *PTR Prentice Hall, Upper Saddle River, NJ*, 28.

Martens, H. (2015). Quantitative big data: where chemometrics can contribute. *Journal of Chemometrics*, 29(11), 563–581. doi:https://doi.org/10.1002/cem.2740. URL `https://analyticalsciencejournals.onlinelibrary.wiley.com/doi/abs/10.1002/cem.2740`.

Pedersen, A.A. (2019). *Optimization Based System Identification for the milliAmpere Ferry*. Master's thesis, Norwegian University of Science and Technology (NTNU), Trondheim, Norway.

Reddy, N.P., Zadeh, M.K., Thieme, C.A., Skjetne, R., Sorensen, A.J., Aanondsen, S.A., Breivik, M., and Eide, E. (2019). Zero-emission autonomous ferries for urban water transport: Cheaper, cleaner alternative to bridges and manned vessels. *IEEE Electrification Magazine*, 7(4), 32–45. doi:10.1109/MELE.2019.2943954.

Roberts, G. (2008). Trends in marine control systems. *Annual Reviews in Control*, 32(2), 263–269. doi:https://doi.org/10.1016/j.arcontrol.2008.08.002. URL `https://www.sciencedirect.com/science/article/pii/S1367578808000278`.

Skjetne, R., Sørensen, M.E.N., Breivik, M., Værnø, S.A.T., Brodtkorb, A.H., Sørensen, A.J., Kjerstad, Ø.K., Calabrò, V., and Vinje, B.O. (2017). AMOS DP Research Cruise 2016: Academic full-scale testing of experimental dynamic positioning control algorithms onboard R/V gunnerus. *Proceedings of the ASME 2017 36th International Conference on Ocean, Offshore and Arctic Engineering*, Volume 1: Offshore Technology. doi:10.1115/OMAE2017-62045. URL `https://doi.org/10.1115/OMAE2017-62045`.

Sørensen, M.E.N. and Breivik, M. (2015). Comparing nonlinear adaptive motion controllers for marine surface vessels. *International Federation of Automatic Control (IFAC)-PapersOnLine*, 48(16), 291–298. doi:https://doi.org/10.1016/j.ifacol.2015.10.295. URL `https://www.sciencedirect.com/science/article/pii/S2405896315021862`. 10th IFAC Conference on Manoeuvring and Control of Marine Craft MCMC 2015, Copenhagen, Denmark.